Journal of Electroanalytical Chemistry 819 (2018) 163–170

Contents lists available at ScienceDirect

Journal of Electroanalytical Chemistry

journal homepage: www.elsevier.com/locate/jelechem

Support induced charge transfer effects on electrochemical characteristics of Pt nanoparticle electrocatalysts

Colleen Jackson[a], Graham T. Smith[a], Matthew Markiewicz[b], David W. Inwood[d], Andrew S. Leach[d], Penny S. Whalley[d], Anthony R. Kucernak[b], Andrea E. Russell[d], Denis Kramer[c], Pieter B.J. Levecque[a,*]

[a] HySA/Catalysis, Catalysis Institute, Department of Chemical Engineering, University of Cape Town, Corner of Madiba Circle and South Lane, Rondebosch 7701, South Africa
[b] Department of Chemistry, Imperial College London, London SW7 2AZ, United Kingdom
[c] Engineering Sciences, University of Southampton, University Road, Southampton SO17 1BJ, United Kingdom
[d] Department of Chemistry, University of Southampton, University Road, Southampton SO17 1BJ, United Kingdom

ARTICLE INFO

Keywords:
Platinum
Boron carbide
Charge transfer
Metal-support interaction
Mass transport
Hydrogen oxidation
X-ray absorption spectroscopy

ABSTRACT

The electrokinetic properties of Pt nanoparticles supported on Carbon (Pt/C) and Boron Carbide-Graphite composite (Pt/BC) are compared over a wide potential range. The influence of the support on the electronic state of Pt was investigated via *in-situ* X-ray Absorption Spectroscopy. Pt d-band filling, determined from XANES white line analysis, was lower and nearly constant between 0.4 and 0.95 V vs. RHE for Pt/BC, indicating more positively charged particles in the double layer region and a delay in the onset of oxide formation by about 0.2 V compared to the Pt/C catalyst, which showed a marked increase in d-band vacancies above 0.8 V vs. RHE. Moreover, Δμ analysis of the XANES data indicated a lack of sub-surface oxygen for the Pt/BC catalyst compared to the Pt/C catalyst above 0.9 V vs. RHE. Additional anion adsorption on the Pt/BC in the double layer region, detected by CO displacement, was also confirmed by XANES analysis of the d-band occupancy. The H_2 oxidation activities of electrodes with low catalyst loadings were assessed under high mass transport conditions using the floating electrode methodology. The metal-support interaction between the Pt and BC support improved the maximum hydrogen oxidation current density by 1.4 times when compared to Pt/C.

1. Introduction

Much current research on polymer electrolyte fuel cells (PEFC) is focused on membrane electrode assembly development since significant challenges remain in increasing kinetic activity, stability, and reducing the cost of catalysts [1]. Typically, Pt nanoparticles supported on carbon are used as catalysts in the hydrogen PEFC anode and cathode, which perform the hydrogen oxidation reaction (HOR) and the oxygen reduction reaction (ORR), respectively. However, the oxidation of the carbon support at high potentials decreases the catalyst lifetime; in addition, Pt dissolution and agglomeration decreases the electrochemically active surface area [2]. Main group carbides have shown promise as alternative support materials with improved Pt catalyst activity and durability reported [3,4].

Recently, some of us have experimentally isolated electronic metal-support interactions for Pt supported on a boron carbide-graphite composites (Pt/BC) compared to commercial Pt/C [4]. This study was carried out using rotating disc electrode (RDE) electrochemical testing, X-ray Photoelectron Spectroscopy (XPS), and X-ray Absorption Spectroscopy (XAS), supported by Density Functional Theory (DFT). The Pt loading on the support surface, particle size, shape and interparticle distances were kept constant in order to investigate electronic metal-support interactions without the effects of other influential factors. The Pt/BC catalysts demonstrated a 50% increase in surface area specific ORR activity at 0.9 V vs. RHE using a standard RDE technique [5] and a ~20% increase in catalyst durability after 6000 cycles in terms of electrochemical surface area (ECSA) retention. The enhanced activity and durability were attributed to changes in electronic metal-support interactions between platinum and the boron carbide-graphite composite support, which were supported by XPS spectra analysis and XANES.

In the study presented herein, we build on this work by further exploring the effects of varying charge transfer between the catalyst and support. The hydrogen oxidation reaction under conditions of high mass transport is used as a surface probe in the oxide region and CO

* Corresponding author.
E-mail address: Pieter.Levecque@uct.ac.za (P.B.J. Levecque).

http://dx.doi.org/10.1016/j.jelechem.2017.10.010
Received 4 August 2017; Received in revised form 28 September 2017; Accepted 3 October 2017
Available online 04 October 2017

displacement was used to investigate interface changes in the double layer region. The observed electrochemical characteristics are correlated to differences in the electronic state of the Pt particles determined in situ using X-ray absorption spectroscopy.

Analysis of the d-band vacancies of the Pt particles as a function of the applied potential was conducted using white line analysis [6]. Additionally, the presence or absence of sub-surface oxygen was explored using the Δμ analysis of the X-ray absorption near edge spectra (XANES) as previously established by Adzic and co-workers [7].

Fundamental investigations of the electrocatalytic performance of catalysts for HOR and ORR are commonly carried out on RDEs. The RDE technique tends to be favoured over PEFC testing [5] as it is cost effective, uses small amounts of catalyst, and the well-defined hydrodynamic conditions and testing protocols tend to give reproducible results [8]. Whilst it is advantageous and convenient to employ the RDE technique, the extrapolation of RDE data to predict performance in PEFCs often leads to inaccurate conclusions, since factors such as oxide coverage, low reactant concentration and differences in water activity are not considered [9,10].

A 'floating electrode' technique recently developed by some of us [11] was tailored to incorporate the advantages of both the RDE method and PEFC measurements to enable studies under high mass transport and low catalyst loading conditions to be performed. Current densities of 600 ± 60 $mA{\cdot}cm_{Pt}^{-2}$ (~5700 $mA{\cdot}cm_{geo}^{-2}$ at 10.15 $\mu g_{Pt}{\cdot}cm^{-2}$) at peak potential for HOR at standard temperature and pressure (STP) were obtained for a commercial Pt/C catalyst. In comparison, RDE measurements for the same catalyst reached limiting current at 2.5 $mA{\cdot}cm_{geo}^{-2}$. The floating electrode results are comparable to kinetic activities for HOR and ORR reported in PEFCs [11,12]. This high mass transport technique allows fundamental studies on HOR and ORR to be carried out in a facile manner, providing data that is comparable to that obtained in more complex PEFC experiments. Additionally, floating electrode studies have established that the HOR is sensitive to surface sites and adlayer morphology and, therefore, can be used as a probe into relative coverages on the platinum surface [13].

2. Experimental

2.1. Catalyst preparation and characterisation

The 20 wt% Pt/C catalysts used in this study were HiSPEC® 3000 commercial catalysts. The 20 eq wt% Pt/BC was prepared in house as reported previously [4]. The full physical characterisation of both catalysts were presented in that previous report and are not repeated. In short, the Pt nanoparticle shapes and particle sizes were the same, however, the electronic properties were found to depend on the nature of the support.

2.2. In-situ XAS

Electrodes were prepared by formation of a catalyst ink which was then coated on to a Teflon coated carbon base layer (Alfa Aesar) and used as the working electrode in an *in-situ* XAS cell [14]. The Pt/C ink formulation consisted of 150 mg of catalyst, 4 ml ultrapure water (Milli-Q 18.2 MΩ·cm), 1 ml isopropanol (Sigma-Aldrich) and 2 ml 5 wt% Nafion. The Pt/BC ink formulation consisted of 150 mg of catalyst, 5 ml ethanol (Sigma-Aldrich) and 2 ml 5 wt% Nafion. Inks were painted on to the carbon layer to give a loading of 0.5 $mg_{Pt}{\cdot}cm_{Pt}^{-2}$. The catalyst coated carbon layer was then hot pressed at 170 °C and 7.8 kPa. All electrodes were flooded prior to use by vacuum filling in ultrapure water. A platinum wire was used as a counter electrode, and $Hg/HgSO_4$ was used as a reference electrode. All potentials have been corrected to RHE using a conversion of 0 V. vs. $Hg/HgSO_4$ = 0.654 V vs. RHE.

The XAS data were collected at the B18 line at the Diamond Light Source, operated with a typical ring energy of 3 GeV with a ring current of 300 mA. Data were collected at the Pt L_3 edge (11 564 eV) and Pt L_2 edge (13 277 eV) in Quick EXAFS (QEXAFS) mode using a Si(111) monochromator and using the ionisation chambers in transmission mode at 298 K. A total of three spectra were averaged for each sample at each potential. Calibration of the monochromator was carried out at both edges using Pt foils. The absorption spectra were modelled out to the fourth Pt shell with Demeter© using Ifeffit© [15] to solve the EXAFS equation.

2.3. CO displacement on RDE

CO displacement was conducted in a 0.1 M $HClO_4$ electrolyte at room temperature in an argon saturated electrolyte. The potential of the working electrode is held for 2 min, thereafter CO is introduced into the electrolyte and the transient current response over time is recorded. A baseline is then assumed from the argon saturated solution current before CO displacement, and the areas under the oxidative and reductive peaks are measured. A platinum counter electrode was used and the reference electrode used was $Hg/HgSO_4$, with potentials reported vs. RHE as described above. Three of the CO displacement curves are shown in Fig. S3 for both catalysts.

2.4. Floating electrode studies

The catalyst layer was prepared as described by Zalitis et al. [11]. Porous polycarbonate track etched (PCTE) membranes (Sterlitech, PCTF0447100) with a pore size of 400 nm and a porosity of 0.125 were coated with a 100 nm gold layer by sputter deposition (Emitech K575X). These gold coated PCTE membranes were then rinsed with propan-2-ol (Sigma-Aldrich, ACS reagent) in a Soxhlet extractor for 8 h, followed by ultra-pure water in the Soxhlet extractor for 8 h. The commercial Pt/C (Alfa Aesar) catalyst ink consisted of 5 mg catalyst, 5 ml ultra-pure water, 1.5 ml propan-2-ol and 25 μl 5 wt% Nafion, 10 μl of this first Pt/C catalyst ink is diluted in 7.7 ml water and 2.3 ml propan-2-ol. The Pt/BC catalyst ink consisted of 2.5 mg catalyst, 0.5 ml ethanol (Sigma-Aldrich, Absolute for HPLC), and 25 μl 5 wt% Nafion, 10 μl of this first Pt/BC catalyst ink was diluted in 10 ml of ethanol. 250 μl of the diluted inks were vacuum filtrated onto 2 mm diameter spots on separate gold coated PCTEs. After deposition of the catalyst layer, a hydrophobic coating of an amorphous fluoropolymer (AF) (DuPont DeNemours, a copolymer of 2,2-bistrifluoromethyl-4,5,difluoro-1,3-dioxile and tetrafluoroethylene with the trade name Teflon AF 2400, 2.1 $\mu g{\cdot}cm_{Geo}^{-2}$) dissolved in Fluorinert FC-40 (Sigma, F9755) was applied to the unmodified side of the gold coated PCTE membrane. The electrodes were then dried at 90 °C for 8 h at 25 mbar before cleaning in ultra-pure water in the Soxhlet extractor for 8 h. Table 1 reports the Pt loadings and roughness factors of the electrodes, where roughness factor was calculated by dividing the Pt active area, determined via CO stripping, by the area of the geometric electrode surface area, using one repeat for each catalyst.

Glassware for the floating electrode measurements was soaked for 8 h in a NoChromix® solution and then boiled in water (Milli-Q, 18.2 MΩ·cm) five times before use. This cleaning procedure was repeated before each electrochemical test. The electrolytes were prepared from Suprapur® grade $HClO_4$ (Merck) and Millipore water (Milli-Q, 18.2 MΩ·cm), whilst the gases used were ≥ 5.8 N (Air Products, BIP PLUS) utilising all stainless high purity regulators (Druva Ultra high purity).

A three electrode setup was employed with a platinum counter

Table 1
Roughness factor and Pt loading on the 20 eq wt% Pt/BC and 20 wt% Pt/C electrodes.

Catalyst	Roughness factor	Pt loading ($\mu gPt{\cdot}cm_{Geo}^{-2}$)
20 wt% Pt/C	1.2 ± 0.1	1.5 ± 0.1
20 eq wt% Pt/BC	0.75 ± 0.1	1.1 ± 0.1

electrode and hydrogen reference electrode, using an AutoLab potentiostat. 1 M $HClO_4$ was used as the electrolyte to decrease the iR drop. The electrolyte was thoroughly purged with N_2 before electrochemical testing was performed and during electrochemical measurements the cell's headspace was continuously purged as diffusion through the electrolyte was considered negligible. Cyclic voltammograms were obtained from 0.05–1.2 V vs. RHE at 100 $mV{\cdot}s^{-1}$ for 50 cycles at room temperature to electrochemically clean the catalyst surface. The scan rate was then changed to 10 $mV{\cdot}s^{-1}$ for two cycles and the potential cycled between 0.05 and 1.1 V vs RHE at room temperature. The cyclic voltammograms are reported in Fig. S4A.

The electrochemical surface area was measured by stripping of an adsorbed CO monolayer. CO was flowed into the cell's headspace for 5 min whilst holding the potential at 0.1 V vs. RHE, N_2 was then flowed in the headspace for 5 min to rid the solution of CO, after which the potential was cycled between 0.05 and 1.2 V vs RHE. The CO stripping voltammograms are reported in Fig. S4B. Due to the 400 nm pore size of the gold coated PCTE, some smaller catalyst particles are lost through the membrane during vacuum filtration. As reported by Zalitis et al. [11], the amount of catalyst which is washed through the membrane is related to catalyst loading on the electrode. Although the amount of catalyst deposited can be determined from H_{upd} measurements, it was found that measurements became difficult at loadings $< 5\ \mu g_{Pt}{\cdot}cm^{-2}$ for commercial HiSPEC 9100 60 wt% Pt/C (Johnson Matthey Fuel Cells) catalyst due to the difficulty of establishing a reliable background. In order to estimate the platinum loading, they utilised a quadratic fit calibrated using the H_{upd} on higher loading electrodes. Rather than using H_{upd} as a measure of surface area, we have used CO-adsorption and stripping, which allows better separation from the background. In the study reported herein, we have assumed a stripping charge of 420 $mC{\cdot}cm_{Pt}^{-2}$ for both types of catalysts.

The HOR activity was measured at a scan rate of 10 $mV{\cdot}s^{-1}$ between 0.05 and 1.1 V vs RHE at room temperature and with flowing H_2 into the cell's headspace. All HOR scans were normalised for electrochemically active surface area and Ohmic drop measured by impedance spectroscopy. Impedance was completed with H_2 in the cell's headspace, at the open circuit potential (OCP) and a frequency of 10 kHz. Error margins on HOR activities were obtained from one repeat for each catalyst.

2.5. Kinetic model and data fitting

A previously published kinetic model by one of us [16] was used to interpret the HOR data under mass transport-free conditions and close to equilibrium (0–0.2 V vs. RHE). The model assumes that the hydrogen reaction is dominated by the Tafel-Volmer reaction:

$$H_{2,surf} + 2S \underset{k_{+T}}{\overset{k_{-T}}{\rightleftarrows}} 2S - H_{ad} \qquad \text{Tafel Step} \tag{1}$$

$$2S - H_{ad} \underset{k_{+V}^{eq}}{\overset{k_{-V}^{eq}}{\rightleftarrows}} 2S + 2H^+ + 2e^- \qquad \text{Volmer Step} \tag{2}$$

where S is a platinum surface site. k_{+T} and k_{-T} are the rate constants associated with the chemical adsorption/desorption of hydrogen on the surface. k_{+V}^{eq} and k_{-V}^{eq} represent the electrochemical rate constant at the equilibrium potential associated with the Volmer step. It is assumed that the electrochemical rate constants vary as the overpotential is modified in a standard electrochemical manner:

$$k_{+V} = k_{+V}^{eq}\, e^{\beta f\eta};\ k_{-V} = k_{-V}^{eq} e^{-(1-\beta)f\eta} \tag{3}$$

where β is the molecular symmetry factor, $f = \frac{F}{RT}$, $\eta = E - E_{eq}$. Under the assumption of a time invariant surface coverage of H_{ads}, but making no other assumptions about which is the slow step, the hydrogen coverage is determined as

$$\theta_{H_{ad}}^{TV}(\eta) = \frac{4B^2 + Z(e^{\beta f\eta} + Be^{-(1-\beta)f\eta}) - \sqrt{16B^2 + (Z(e^{\beta f\eta} + Be^{-(1-\beta)f\eta}))^2 + 8BZ(Be^{\beta f\eta} + e^{-(1-\beta)f\eta})}}{4(B^2 - 1)}$$
$$B = \sqrt{\frac{a_{H2}k_{+T}}{k_{-T}}},\ Z = \frac{k_{+V}^{eq}}{k_{-T}} \tag{4}$$

where $\theta_{H_{ad}}{}^{TV}$ is the coverage of hydrogen, and B and Z are dimensionless ratios of the rate constants introduced in order to make the equations more tractable. Utilising the hydrogen coverage, it is then possible to determine the current density as a function of overpotential.

$$\frac{j^{TV}(\eta)}{k_{-T}} = FZ\left(\theta_{H_{ad}}^{TV}(\eta)e^{\beta f\eta} - B(1 - \theta_{H_{ad}}^{TV}(\eta))e^{-(1-\beta)f\eta}\right) \tag{5}$$

where $j^{TV}(\eta)$ is the electrochemical current density as a function of overpotential.

For each catalyst the function was fit to two independent HOR curves (independent means produced using separately produced electrodes) in order to reduce statistical uncertainty. Fitting was performed in Excel fitting the curve using three parameters: B, Z, and k_{-T} whilst fixing $\beta = 1/2$. β was fixed to this value as a previous study gave a value very close to 1/2 for the Tafel Volmer mechanism. Using the fit parameters, the values of k_{+T}, k_{+V}^{eq}, and k_{-V}^{eq} can be determined by substitution. The fits were performed using the GDG non-linear solver with Multistart and a population of 100, using the method described by Kucernak & Zalitis [16]. This approach statistically determines if the global minimum is found by randomly sampling the result using a large population of starting parameters. The fitted (2 samples) and measured HOR curves are compared in Fig. 6. The fits are only performed for the 1st 200 mV of the curve, as the fitting model used does not take into account the shutdown of the HOR at potentials greater than the PZTC due to anion/oxide adsorption. This effect has been taken into account in a later model, but would add further fitting parameters [21].

3. Results

3.1. In-situ XAS

In-situ XANES at the Pt L_3 and L_2 – edges for the 20 eq wt% Pt/BC and 20 wt% Pt/C catalysts at each potential are shown in Fig. 1, which have been presented to highlight the potential dependence of the white line at the Pt L_3 edge and variations in the post-edge features at the Pt L_2 edge. An increase in the L_3 and L_2 white line intensity as potential increased is seen for both the Pt/BC and Pt/C catalysts.

The XANES at the $L_{2,3}$ edges originate from exciting 2p core states. The L_2 edge arises from the 2p J = 1/2 core states, and the L_3 X-ray absorption edge arises from the 2p J = 3/2 core states, excited to vacant d-states. Comparison of the spectra for the two edges enables assessment of the d-band vacancy per Pt atom using a method described by Mansour et al. [6]. The d-band vacancies calculated using this method, assuming a bulk Pt d-band vacancy of 0.3 as theoretically calculated by Brown et al. [17], are reported in Fig. 2. The d-band vacancies of the 20 wt% Pt/C catalyst increased significantly as potential increased from approximately 0.8 V vs. RHE. The d-band of the 20 eq wt% Pt/BC was less occupied at lower potentials than found for the Pt/C catalyst. However, the Pt/BC d-band occupancy is significantly less sensitive to potential than seen for Pt/C and remained unchanged until approximately 1.0 V vs. RHE.

Subtle changes to the XANES L_3 region due to adsorbate formation and place exchange on the platinum surface can be more closely studied by the Δμ technique, which involves subtracting two XANES spectra of the same sample at different potentials from each other [7]. The subtraction of the two spectra removes the bulk metal-metal interactions if the metal-metal coordination of the particles is unchanged (implying no significant particle shape change or extensive oxide formation) over the

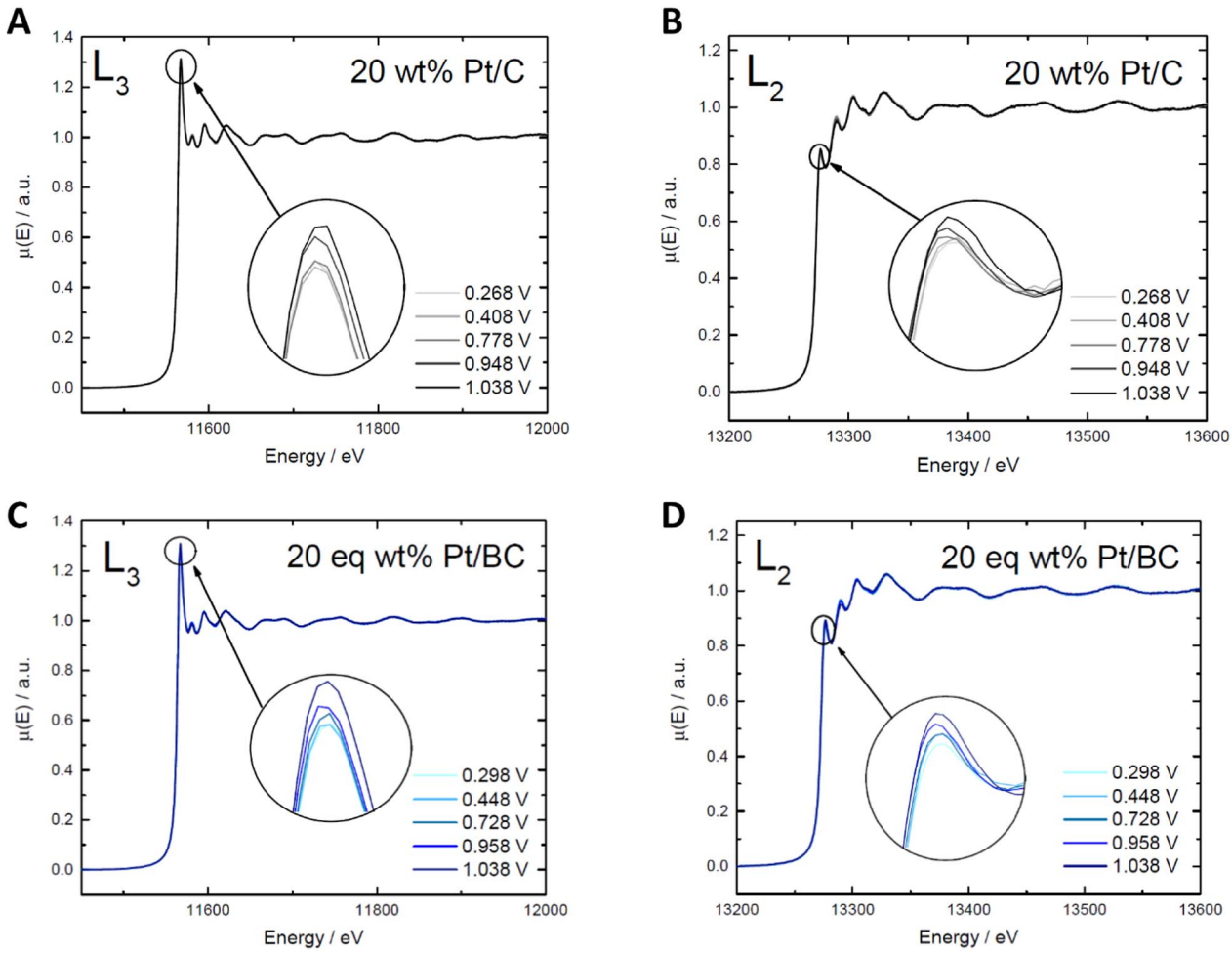

Fig. 1. The X-ray adsorption spectra for the (A) Pt L_3 edge and (B) Pt L_2 edge of the 20 wt% Pt/C catalyst and (C) Pt L_3 edge and (D) Pt L_2 edge of the 20 eq wt% Pt/BC catalyst. Circles showing the expansion of the leading peak are all performed at the same magnification. The intensity of the post edge feature (white line) increases with potential for both catalysts.

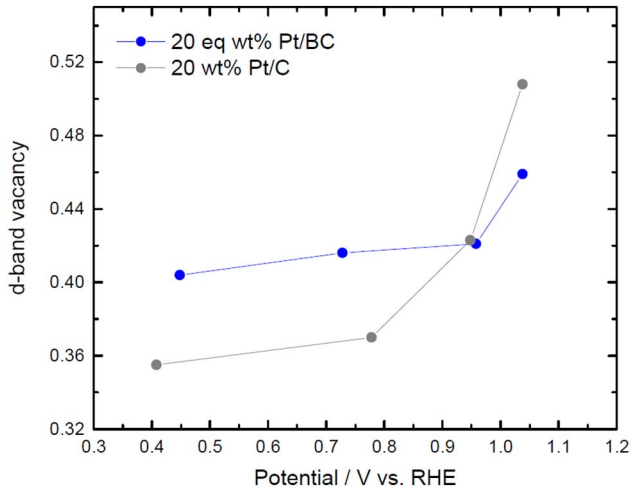

Fig. 2. d-Band vacancy at different potentials on the Pt/C and Pt/BC catalysts.

potential range explored, and, therefore, isolates the surface changes due to adsorbates [18]. These assumptions were verified by analysis of the EXAFS data (presented in the Supplementary Information Figs. S1–2, and Tables S1–2). No changes in Pt—Pt coordination numbers or Pt—Pt distances within the error in the fits were observed for the first four coordination shells over the explored potential range.

The Δμ spectra were calculated using the spectra obtained in the double layer region as the reference, where it is assumed that the Pt surface is free of oxides, at 0.408 V and 0.448 V for the Pt/C and Pt/BC catalysts, respectively. The potential difference between the Pt/C (0.408 V) and Pt/BC (0.448 V) is not significant to d-band occupancy, since these are in the double layer region. Fig. 3A details the Δμ (0.778), Δμ (0.948) and Δμ (1.038) curves of the Pt/C XANES spectra. The Δμ curves display a peak below the edge energy (E_0) at 11565 eV followed by a positive peak above E_0 at 11570 eV. The Δμ (0.728), Δμ (0.958) and Δμ (1.038) curves of the Pt/BC XANES spectra are shown in Fig. 3B. Whilst the positive peak at energies above the edge is present in the difference spectra for both catalysts, the initial negative Δμ response, seen for Pt/C (Fig. 3A), is not seen on the Pt/BC Δμ curves (Fig. 3B). The Δμ (1.038) peak of the Pt/BC is approximately twice as large as the Δμ (1.038) peak of the Pt/C.

3.2. CO displacement versus potential

CO displacement measurements were conducted over a wide potential range. There are notable changes to the gradient of the charge density curves normalised for platinum surface area versus potential for the different catalysts, displayed in Fig. 4. The curves show a positive displacement charge at low potentials, attributed to the displacement of H species. At higher potentials, a negative displacement charge is observed and is understood as an indication of anion adsorption and to a lesser degree an interaction with interfacial water [19,20] in the double layer region. The charge displacement gradient observed for Pt/BC is steeper than that for Pt/C, with a larger minimum charge of

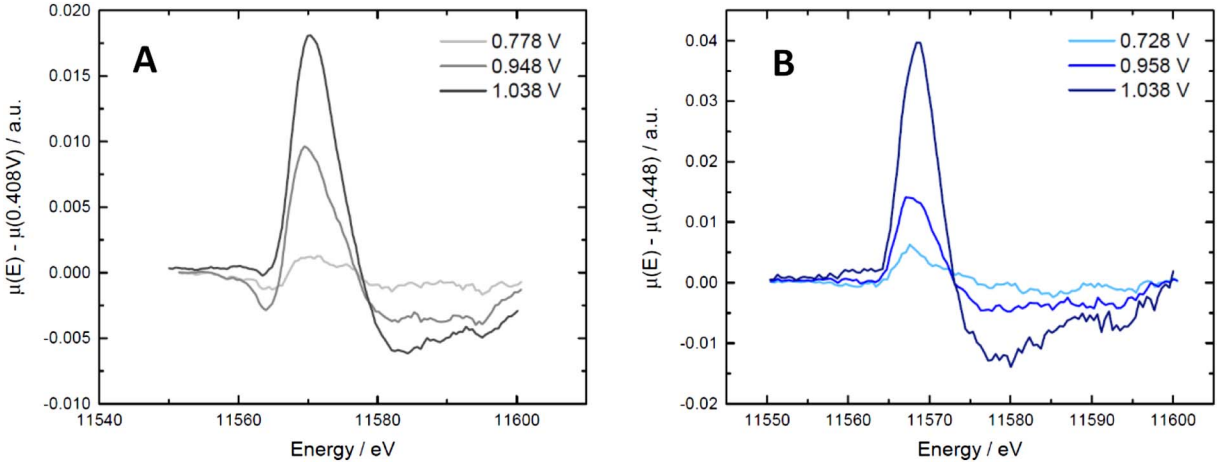

Fig. 3. The calculated Δμ curves at different potentials on the (A) Pt/C and (B) Pt/BC catalysts. The reference spectrum was obtained at 0.408 V vs RHE for the Pt/C and 0.448 V vs RHE for the Pt/BC catalysts. The peak at 11570 eV in the difference spectra increases with sample potential for both catalysts.

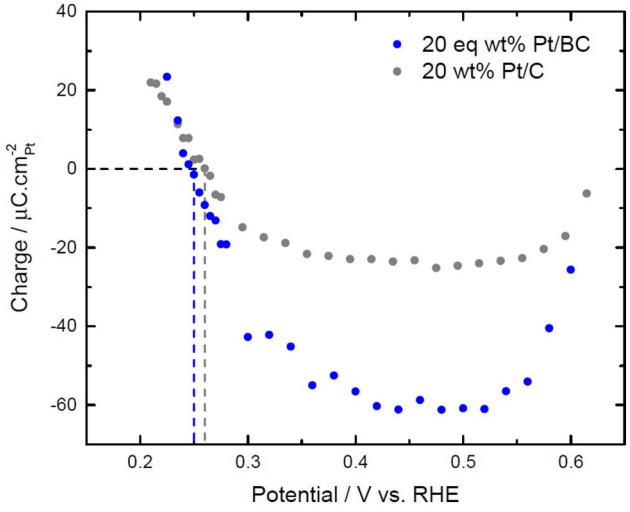

Fig. 4. The CO displacement charge density curves for the 20 wt% Pt/C and 20 eq wt% Pt/BC catalysts. The vertical dashed lines indicated the potential of total zero total charge (ptzc).

~600 mC·m^{-2}_{Pt} compared to Pt/C (~200 mC·m^{-2}_{Pt}). At potentials above ~0.5 V vs. RHE, a reduction of displacement charge is seen because of the onset of CO oxidation to CO_2. The values for the potential of total zero charge (ptzc) are 0.25 and 0.26 V vs. RHE on the Pt/BC and Pt/C catalysts, respectively.

3.3. Hydrogen oxidation reaction under high mass transport conditions

The HOR was studied on the 20 wt% Pt/C and 20 eq wt% Pt/BC catalysts under high mass transport and low catalyst loading conditions. Fig. 5 shows the surface area specific HOR activity, normalised by using the ECSA obtained from the CO stripping measurements. Starting from equilibrium at 0 V vs. RHE, the Faradaic current first increases, then passes through maxima, and finally decreases at high potential. Peaks observed in Fig. 5A between 0.20 and 0.42 V vs. RHE have previously been ascribed to different Pt sites [21], followed by an asymptotic decrease at potential above 0.42 V vs. RHE. Additionally, a hysteresis occurs between the forward and reverse scans. Table 2 reports the mass specific and surface area specific current densities for these catalysts. A maximum surface area specific current density of 646 ± 24 mA·cm^{-2}_{Pt} is obtained on the Pt/BC catalyst, which is approximately 1.4 times that obtained on the Pt/C catalyst at 459 ± 22 mA·cm^{-2}_{Pt} although somewhat less than that obtained on HiSpec 9100 60 wt% Pt/C catalyst (ca. 650 mA·cm^2) [11].

4. Discussion

4.1. Catalyst state of charge at intermediate potentials

The d-band vacancy over a wide potential range is reported in Fig. 2. Firstly, the d-band vacancy of the commercial Pt/C catalyst follows that reported by Mukerjee and co-workers [22,23] for similar catalysts. The d-band vacancy of the Pt/C catalyst increases slightly between 0.4 and 0.8 V vs RHE. This increase in d-band vacancy is attributed to an increasing amount of OH_{ads} species and anion adsorption on the surface of Pt [22,23]. A significantly more vacant d-band is calculated for the Pt/BC catalyst in the double layer region compared to Pt/C. This indicates more positively charged Pt particles at a given potential in the potential range between about 0.4 to 0.8 V vs RHE for Pt/BC. We have argued previously [4] that a lower work function of the boron carbide support should result in a decrease in the potential of zero charge (pzc) of the Pt/BC catalyst when compared to Pt/C [4]. This is tentatively understood to imply additional anion adsorption as well. CO displacement, as described by Climent et al. [24], is a method for determining the potential of total zero charge (ptzc) on a platinum surface. CO displaces weakly adsorbed anions and cations completely from the surface, due to the strong adsorption of CO onto Pt. It is assumed that CO adsorption on the surface results in zero net charge passing through the interface. The subsequent transient charge, therefore, is a result of displacement of the initially adsorbed anion and cation species. In addition, interfacial water has shown to interact strongly with CO-free Pt surfaces and may also influence CO displacement charges [19]. The displacement charge is zero at the ptzc, assuming that no other reactions take place and the remaining charge on the surface after CO adsorption can be neglected. Therefore, the CO displacement charge on the catalysts at potentials above the ptzc is largely attributed to the displacement of anions and some contribution of interfacial water. The capacitance contribution from double layer charging of electrolyte dipoles is ~15 μF·cm^{-2}_{Pt} measured on a Pt(111) surface in 0.1 M $HClO_4$ electrolyte [19]. This capacitance translates to charge density of the order of 10 μC·cm^{-2}_{Pt} in the double layer region (assuming a potential of zero charge for clean Pt of ~1 V vs RHE [19]). Therefore, the expected contribution from double layer polarisation due to changes in pzc to the charge density is significantly smaller than what is measured at 0.5 V vs. RHE on the Pt/BC catalyst of ~60 μC·cm^{-2}_{Pt} and thus the measured charge density is predominately attributed to anion absorption.

Fig. 4 confirms the assertions from d-band vacancy of a larger coverage of anions on the surface of Pt/BC compared to Pt/C in the double layer potential region (0.4–0.5 V vs. RHE). The displacement

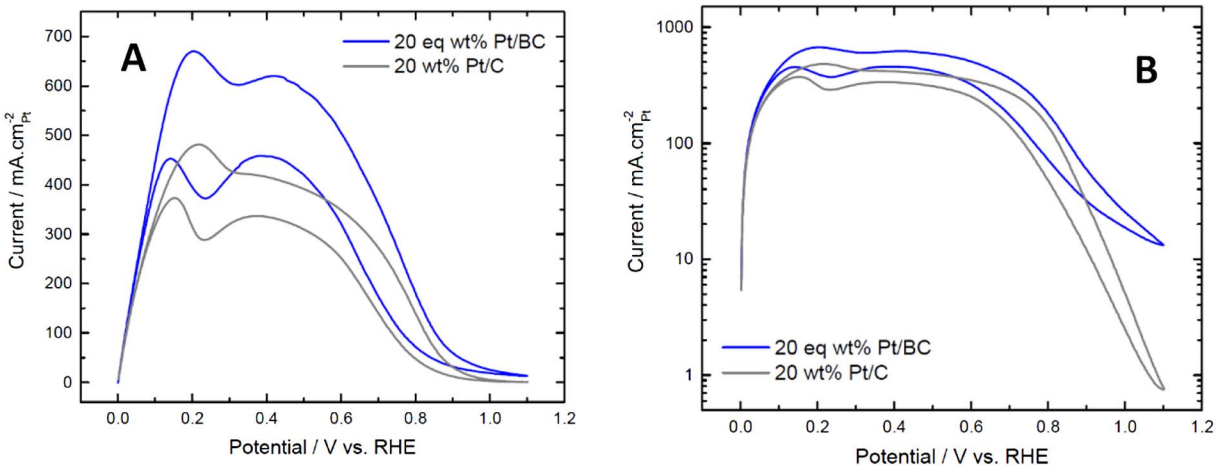

Fig. 5. (A) Plots of H_2 oxidation on 20 eq wt% Pt/BC and 20 wt% Pt/C catalysts in a 1 M $HClO_4$ electrolyte solution at room temperature and a scan rate of 10 mV.s^{-1} and (B) the corresponding logarithmic. Catalyst loadings were 1.5 ± 0.1 μgPt·cm$^{-2}_{Geo}$ and 1.1 ± 0.1 μgPt·cm$^{-2}_{Geo}$ for Pt/C and Pt/BC, respectively.

Table 2
Maximum hydrogen oxidation activities for the 20 eq wt% Pt/BC and 20 wt% Pt/C catalysts.

Catalyst	Mass activity (A·mg$^{-1}_{Pt}$)	Surface area specific activity (mA·cm$^{-2}_{Pt}$)
20 wt% Pt/C	380 ± 18	459 ± 22
20 eq wt% Pt/BC	437 ± 16	646 ± 24

charge is almost 3 × larger on Pt/BC and corresponds to roughly $\frac{1}{3}e^-$ per surface Pt. This indicates a very substantial coverage given the size of likely anions (ClO_4^- from the electrolyte and SO_3^- from the ionomer). CO displacement, therefore, confirms the conclusion reached from XANES that Pt/BC is more positively charged at intermediate potentials with stronger anion adsorption approaching full coverage.

4.2. Surface oxidation at high potentials

The Pt d-band vacancy at higher potentials change more strongly as the adsorbed OH_{ads} anions are replaced by more strongly adsorbing oxygen. This strongly adsorbing oxygen leads to a non-linear increase in d-band vacancy at higher potentials as seen in Fig. 2. This is seen for both catalysts. The delay of about 0.2 V seen for Pt/BC, however, indicates a lower tendency of Pt to oxidise if supported on BC relative to being supported on C.

Similarly to the Pt/C curves in Fig. 3A, the Pt/BC Δμ curves shown in Fig. 3B have a positive peak which is attributed to O or OH adsorbates on the Pt surface. The positive peak generally increases with increasing potential and is attributed to an increased coverage with oxygen species at the surface on both catalysts [7]. The Δμ technique also showed an initial negative response on the Pt/C curves. This feature has previously been correlated with sub-surface oxygen due to platinum place-exchange [18,25]. Sasaki et al. [7] confirmed this relationship between the negative peak in XAS and sub-surface oxygen by X-ray Diffraction (XRD) analysis. The absence of the negative peak for Pt/BC is noteworthy and ascribed to a smaller tendency to form sub-surface oxygen on the Pt/BC catalyst, broadly in agreement with the lower tendency of Pt to oxidise on BC, which might indicate less strongly bound oxygen on the Pt nanoparticles when supported on the boron carbide-graphite composite. The Δμ(1.038) peak of the Pt/BC catalyst shows a larger peak height, of approximately twice that of Pt/C. This difference is another manifestation of the effects of sub-surface oxygen for the Pt/C catalyst and arises from the fact that these are difference spectra. The shift to higher energy in the spectrum as the potential increases that gives rise to the negative peak at 11565 eV for the Pt/C spectrum also decreases the intensity in the difference spectra for the peak at 11570 eV.

4.3. HOR at low potentials

The HOR results shown in Fig. 5 are in agreement with previous studies of HOR on a Pt/C catalyst under high mass transport and low catalyst loading conditions [11,12]. Zalitis et al. [26] thoroughly investigated the HOR current density behaviour and underlying causes under different experimental conditions; this was followed up by a study utilising theoretical modelling yielding further insights [16]. Parameters such as electrolyte, electrolyte concentration, roughness factors, gas partial pressures, temperature and scan limits were investigated for the influence on hydrogen oxidation and oxygen reduction reactions, obtaining a maximum surface area specific current density of 600 ± 60 mA·cm$^{-2}_{Pt}$ for a commercial 60 wt% Pt/C catalyst. In those studies, it was proposed that the two peaks are correlated to reactivity at two different surface sites, edges or Pt atoms with low coordination numbers (low potential peak) and facets (higher potential peak) [26]. The initial current density drop after the higher potential peak was attributed to anion adsorption impeding the HOR. This hindrance of the reaction is expected to be most influential at potentials between the potential of total zero charge (ptzc) and ~0.8 V vs. RHE, where adsorbed anions are displaced by more strongly adsorbed oxides further impeding the HOR [26].

Noteworthy differences in absolute HOR activity are observed across the entire potential range. Fig. 5 and Table 2 show that the maximum surface area specific current densities are approximately 1.4 times larger on the 20 eq wt% Pt/BC catalyst when compared to the 20 wt% Pt/C catalyst.

The HOR data in the potential range 0–0.2 V vs. RHE (i.e. below the ptzc, where anion adsorption is expected to be negligible) was fitted using the theoretical model derived by Kucernak and Zalitis [16] to gain further insights (see Experimental for details, Fig. 6 for fits and Table S3 for complete list of derived parameters including limiting current densities for the Tafel step, exchange current densities for the hydrogen reaction, equilibrium coverage of H_{ads} and free energy of adsorption of hydrogen). It was found that all fitted parameters were in a factor of four of those determined for a different Pt/C catalyst previously reported (see Table S3). The dimensionless parameter B and Z and k_{-T} were the fit parameters, and from these parameters the rate constants for the Tafel and Volmer steps (described in Eqs. (1) and (2), respectively) were then extracted. Table 3 presents the values determined under equilibrium conditions, where k_{+T} and k_{-T} are associated with the forward and reverse Tafel steps, respectively, and k_{+V}^{eq}

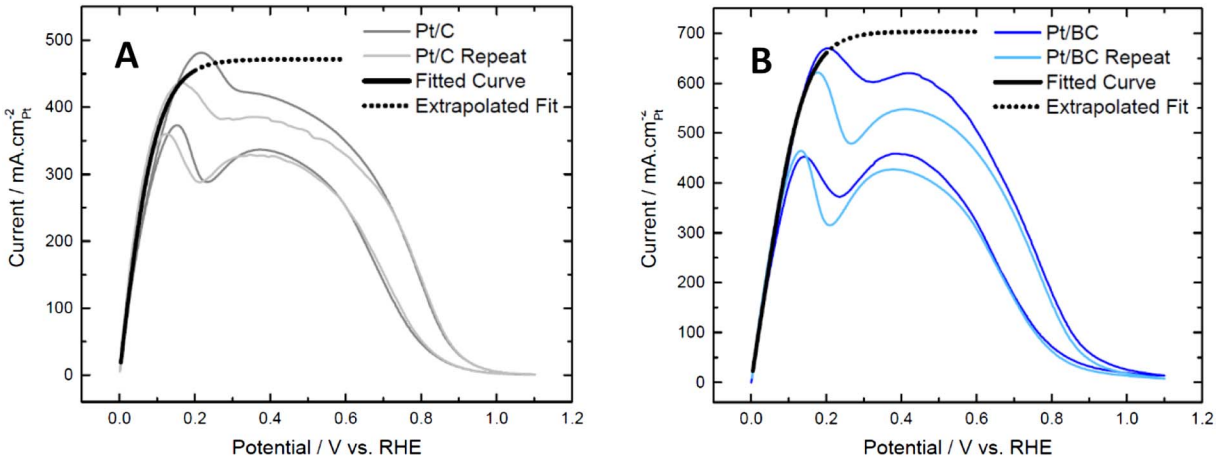

Fig. 6. HOR curves for (A) Pt/C and (B) Pt/BC catalysts with the fitted model in the potential range of 0–0.2 V vs. RHE (solid line) and the model at potentials beyond the fitted region, 0.2–0.6 V vs. RHE (dashed line).

Table 3
Rate constants of the Tafel and Volmer steps for hydrogen oxidation on 20 wt% Pt/C and 20 eq wt% Pt/BC derived from the fit of the experimental data (see Table S3). The molecular symmetry factor, β, is fixed to 1/2 (see [16]). The fitted and measured HOR curves were reported in Fig. 6, the residual sum of squares for the fitting is calculated to be within 1% of the experimental data.

Catalyst	H_2 adsorption $10^6\,k_{+T}$/ mol·cm^{-2}·s^{-1}	H_{ad} combination $10^6\,k_{-T}$/ mol·cm^{-2}·s^{-1}	H_{ad} oxidation $10^6\,k_{+V}^{eq}$/ mol·cm^{-2}·s^{-1}	H^+ reduction $10^6\,k_{-V}^{eq}$/ mol·cm^{-2}·s^{-1}
20 wt% Pt/C	2.44	4.96	5.45	3.82
20 eq wt% Pt/BC	3.65	9.57	4.71	2.91

and k_{-V}^{eq} are associated with the forward and reverse Volmer steps, respectively. The fitting of k_{-T} contained a high degree of uncertainty since the results did not extend into the hydrogen evolution region. All parameters are included in Table S3 where the data is also compared to the values for a 60 wt% Pt/C catalyst taken from [16]. Table 3 shows the adsorption of hydrogen to be rate limiting above the ptzc (i.e. at potential significantly positive of the equilibrium potential) for both the Pt/C and Pt/BC catalysts giving rise to anodic specific limiting currents of 472, and 794 mA·cm^{-2} respectively. These anodic limiting currents correspond to a hydrogen turnover frequency of 1100 and 1700 s^{-1} for each surface platinum atom. The hydrogen adsorption rate constant on Pt/BC is determined to be approximately 1.5 times faster than on Pt/C, indicating that the observed higher HOR activity at larger overpotentials on Pt/BC is due to a more facile Tafel step.

This is broadly in agreement with theoretical work by Nørskov [27]. Modelling by Nørskov [27] found the Pt—H adsorption state to be the highest energy state ($\Delta G_{H_*} = +0.03$ eV) at high coverages of Pt(111) fcc sites. Therefore, the adsorption of hydrogen (Tafel step) is expected to be the rate limiting step of the hydrogen oxidation reaction at high H coverages. Changes in the d-band filling (and therefore d-band centre relative to the Fermi level) are suggested to have consequences for covalently stabilised reaction intermediates following Nørskov's d-band theory [28], although electrostatics and other effects should also be considered [29]. In any case, the faster rate of adsorption of H_{ad} at equilibrium suggests a decrease in the Pt—H energy state on the Pt/BC catalysts due to electronic metal-support interactions. However, the work of Nørskov [27] also indicated that H is more strongly adsorbed at low H coverage, which could indicate a change in the rate limiting step above ptzc. Thus, more work is needed to fully understand the HOR characteristics above the ptzc.

The relationship between work function and M—H bond (where M is a metal) was reported by Trasatti [30], showing an increase in M—H bond strength with a decrease in the work function of the metal. This is in accordance with the results presented, as the metal-support interaction on Pt/BC is suggested to decrease the work function of the catalyst compared to Pt/C, thus increasing the Pt—H bond strength and subsequently decreasing the activation energy of the Tafel Step.

Interestingly, the 20 wt% Pt/C and 20 eq wt% Pt/BC catalysts demonstrate qualitatively the same HOR behaviour, with a loss in current density from 0.42–0.8 V vs. RHE of approximately 70% on both catalysts. As this has previously been attributed to anion adsorption blocking Pt sites for HOR, it is not immediately clear why the relative loss in HOR activity seems to be largely insensitive to the larger anion coverage on Pt/BC that we inferred from CO displacement. The anion adsorption in this potential range include SO_3^- groups, present due to the Nafion on the electrode, and ClO_4^- in the electrolyte. There is the possibility of specifically adsorbed anions carrying different charge on the surface of Pt/C than on Pt/BC, which introduces some uncertainty for the interpretation of CO displacement charges. At the same time, changes in the catalyst state of charge can be expected to not only influence the binding energy of charged adsorbates due to electrostatics, but will also bear consequences for reaction intermediates as discussed above. It is, therefore, not immediately clear how these competing effects affect overall activity. Further work is, therefore, needed to disentangle contributions from anion adsorption and reaction intermediates to overall HOR activity between the ptzc and the oxide region.

4.4. HOR at high potentials

Turning to potentials above 0.8 V vs. RHE, the HOR is adversely impacted by oxide species at both Pt/C and Pt/BC. The Pt/BC catalyst, however, shows a better retention of HOR activity, leading to an order of magnitude higher HOR current at 1.1 V vs RHE compared to Pt/C, as clearly shown in Fig. 5. The HOR improvement at 1.1 V vs. RHE on the 20 eq wt% Pt/BC is reportedly due to less oxide formation at these potentials, and thus more free Pt sites for hydrogen oxidation to occur [16]. This is in agreement with the observed trends in d-band vacancies on the 20 eq wt% Pt/BC shown in Fig. 2, which also suggested less oxide formation or strongly bonded oxygen species at high potentials.

5. Conclusion

The influence of charge transfer due to electronic metal-support interactions on electrochemical characteristics of supported Pt nanoparticles was investigated over a wide range of potentials. *In-situ* X-ray absorption spectroscopy demonstrated significantly different responses to potential changes and adsorbates on Pt/BC when compared to Pt/C catalysts. The d-band vacancy of the Pt/BC catalyst in the double layer

region is larger than that of the Pt/C catalyst; this was correlated with increased anion adsorption at potentials positive of the ptzc. Additionally, a 0.2 V delay in oxide formation on the Pt/BC compared to Pt/C was observed.

The Δμ technique, employed to analyse the XAS spectra, enhanced the sensitivity of the spectra to enable detection of − OH adsorption on the Pt surface, and the subsequent vulnerability of the Pt nanoparticles when supported on carbon to disruption by the presence of sub-surface oxygen. This sub-surface oxygen was not detected on the Pt/BC catalysts, suggesting a platinum surface that is more stable when supported on the boron carbide-graphite composite support material.

The Hydrogen Oxidation Reaction (HOR) studies under high mass transport and low catalyst loading conditions showed enhanced activity on the Pt/BC catalyst, when compared to the Pt/C catalyst. This increase in activity is attributed to changes in the Tafel step. Pt supported on BC led to a faster rate of adsorption of H_{ad} at equilibrium, suggesting an increase in Pt−H adsorption energy on Pt/BC catalysts close to equilibrium and, therefore, enhanced HOR activity on Pt/BC. Additionally, less oxide formation at higher potentials was noticed in HOR activity at 1.1 V vs. RHE on the 20 eq wt% Pt/BC, confirming the resilience of Pt/BC against sub-surface oxidation as asserted from the d-band vacancy at high potentials.

Acknowledgements

This work was largely supported by the Royal Society in the form of a Royal Society-Newton Advanced Fellowship (P.L.; grant no. NA140367). C.J. thanks the University of Cape Town for financial support through the UCT PhD Mobility Grant. D.K., G.T.S. and A.R.K. thank the EPSRC H2FC SUPERGEN (grant no. EP/J016454/1) for financial support. G.T.S. thanks the HySA/Catalysis Programme for a postdoctoral fellowship. D.K. acknowledges support from STFC (ST/K00171X/1 and ST/N002385/1). P.L., A.E.R. and D.K. thank the HEFCE Newton Fund Official Development Assistance allocation 2016/17 for financial support. Facilities use was supported by the HySA/Catalysis Centre of Competence (UCT), The Chemistry Department (Imperial College London) and the Department of Chemistry (UoS). Additionally, we thank Diamond Light Source for instrument access on B18 (experiment number SP14146-1) and the station scientists Giannantonio Cibin and Diego Gianolio for their assistance.

Appendix A. Supplementary data

Supplementary data to this article can be found online at https://doi.org/10.1016/j.jelechem.2017.10.010.

References

[1] T.J. Schmidt, ECS Trans. 45 (2) (2012) 3–14.
[2] Y. Shao, G. Yin, Y. Gao, J. Power Sources 171 (2) (2007) 558–566.
[3] H. Lv, S. Mu, N. Cheng, M. Pan, Appl. Catal. B Environ. 100 (1–2) (2010) 190–196.
[4] C. Jackson, G.T. Smith, D.W. Inwood, A.S. Leach, P.S. Whalley, M. Callisti, T. Polcar, A.E. Russell, P. Levecque, D. Kramer, Nat. Commun. 8 (2017) 15802.
[5] K.J.J. Mayrhofer, D. Strmcnik, B.B. Blizanac, V. Stamenkovic, M. Arenz, N.M. Markovic, Electrochim. Acta 53 (7) (2008) 3181–3188.
[6] A.N. Mansour, J.W. Cook, D.E. Sayers, J. Phys. Chem. 88 (11) (1984) 2330–2334.
[7] K. Sasaki, N. Marinkovic, H.S. Isaacs, R.R. Adzic, ACS Catal. 6 (1) (2016) 69–76.
[8] F. Maillard, S. Pronkin, E.R. Savinova, Fuel Cell Catalysis, John Wiley & Sons, Inc., 2009, pp. 507–566.
[9] J.P. Owejan, J.E. Owejan, W. Gu, J. Electrochem. Soc. 160 (8) (2013) F824–F833.
[10] T.A. Greszler, D. Caulk, P. Sinha, J. Electrochem. Soc. 159 (12) (2012) F831–F840.
[11] C.M. Zalitis, D. Kramer, A.R. Kucernak, Phys. Chem. Chem. Phys. 15 (12) (2013) 4329–4340.
[12] C.M. Zalitis, D. Kramer, J. Sharman, E. Wright, A.R. Kucernak, ECS Trans. 58 (1) (2013) 39–47.
[13] G.J. Offer, Quantitative Measurement of Species Adsorbed on Electrocatalysts During Fuel Cell Relevant Reactions, Ph.D. Thesis Imperial College London, 2007.
[14] A.M. Wise, Characterisation of Bimetallic Alloy and Core-shell Electrocatalysts, Ph.D. Thesis University of Southampton, 2012.
[15] B. Ravel, M. Newville, J. Synchrotron Radiat. 12 (2005) 537–541.
[16] A.R. Kucernak, C. Zalitis, J. Phys. Chem. C 120 (20) (2016) 10721–10745.
[17] M. Brown, R.E. Peierls, E.A. Stern, Phys. Rev. B 15 (2) (1977) 738–744.
[18] M. Teliska, W.E. O'Grady, D.E. Ramaker, J. Phys. Chem. B 109 (16) (2005) 8076–8084.
[19] A. Cuesta, Surf. Sci. 572 (1) (2004) 11.
[20] J. Huang, A. Malek, J. Zhang, M.H. Eikerling, J. Phys. Chem. C 120 (25) (2016) 13587–13595.
[21] C.M. Zalitis, A.R. Kucernak, J. Sharman, E. Wright, J. Mater. Chem. A (2017) in press https://doi.org/10.1039/c7ta05543a.
[22] S. Mukerjee, S. Srinivasan, M.P. Soriaga, J. McBreen, J. Electrochem. Soc. 142 (5) (1995) 1409–1422.
[23] S. Mukerjee, S. Srinivasan, M.P. Soriaga, J. McBreen, J. Phys. Chem. 99 (13) (1995) 4577–4589.
[24] V. Climent, R. Gomez, J.M. Orts, A. Rodes, A. Aldaz, J.M. Feliu, Interfacial Electrochemistry: Theory: Experiment, and Applications, Taylor & Francis, New York, 1999.
[25] T.M. Arruda, B. Shyam, J.M. Ziegelbauer, S. Mukerjee, D.E. Ramaker, J. Phys. Chem. C 112 (46) (2008) 18087–18097.
[26] C.M. Zalitis, J. Sharman, E. Wright, A.R. Kucernak, Electrochim. Acta 176 (2015) 763–776.
[27] J.K. Nørskov, T. Bligaard, A. Logadottir, J.R. Kitchin, J.G. Chen, S. Pandelov, U. Stimming, J. Electrochem. Soc. 152 (3) (2005) J23–J26.
[28] J.K. Nørskov, T. Bligaard, J. Rossmeisl, C.H. Christensen, Nat. Chem. 1 (1) (2009) 37–46.
[29] P. Quaino, F. Juarez, E. Santos, W. Schmickler, J. Nanotechnol. 5 (2014) 846–854.
[30] S. Trasatti, J. Electroanal. Chem. Interfacial Electrochem. 39 (1) (1972) 163.